Aerodynamic Calculations Related To Tethered Sub-Satellite Experiments

Final Report

NASA Research Grant NAG-1-878-

Analysis of Aerothermodynamic Experiments

that may be Conducted with Tethered Satellites

Principal Investigator:

J. Leith Potter

Period Covered:

1 June 1988 to 31 July 1991

Vanderbilt University

Department of Mechanical Engineering

Station B, Box 1592

Nashville, TN 37235

SUMMARY

This report presents the results of four aerodynamic studies that were in support of a broader, preliminary inquiry concerning the potential use of downward-deployed tethered sub-satellites for in-flight aerothermodynamic research. There are a multitude of questions regarding the general tethered satellite concept and the present report addresses only a few of these. A method for estimating drag and local surface pressure and shear on orbiting or re-entering bodies is described, and examples based on the planned TSS-2 are given. The problems of pressure measurement are explored, taking into account thermal transpiration, lag time, and the disturbed flow field created by the satellite body. The performance of an aerodynamic stabilizer, a ring-tail design, is calculated and its influence on satellite motion is illustrated. A method for optimizing future satellite shapes for desired aerodynamic properties in transitional rarefied flow with given geometric constraints is proposed and examples are shown.

NOMENCLATURE

A	reference area
C	chord of stabilizer (Fig. 8)
C_D	drag coefficient
C_L	lift coefficient
C_M	moment coefficient
C_f	friction coefficient
C_p	pressure coefficient
d	diameter
E	fraction of specularly reflected molecules
H	enthalpy $(m/s)^2$
h	altitude (km)
Kn	Knudsen number
L	tail moment arm (Fig. 8)
p	pressure
$p_l(x)$	static pressure at station x
$p_t(x)$	impact pressure at station x
p_∞	freestream pressure
R	radius of satellite and tail
S	molecular speed ratio
T	temperature
t	time
U	velocity
x	distance upstream from stagnation point
α	angle of attack
β	see Fig. 8
δ	see Fig. 11
θ	see Fig. 8
λ	mean free path
υ	kinematic viscosity

Subscripts

fm	free molecular	∞	freestream
i	inviscid flow	w	wall

1. INTRODUCTION

The usefulness and feasibility of aerothermodynamic experimentation using downward-deployed, tethered, sub- satellites have been discussed for several years, cf. Refs. 1- 6. The tethered satellite system (TSS) identifies a concept involving a vehicle, such as the NASA Space Shuttle Orbiter, in low Earth orbit at, say, 220-230 km altitude, towing a small, instrumented sub-satellite which is deployed by a tether as much as 100-120 km downward. Some applications of this concept involve upward deployment, but we are only concerned with downward deployment here. In this fashion, the atmospheric conditions and aerothermodynamic phenomena at 100- 130 km would be made accessible for study over extended times. The excessive aerodynamic drag and related propulsion requirement that excludes larger vehicles from prolonged operations at these lower altitudes would be avoided. There is much interest and value in both the atmospheric data and the aerothermodynamic research results expected from such experiments.

Many of the essential points in regard to the conditions imposed upon aerothermodynamic research application of a tethered satellite system (TSS) orbiting at 100-130-km altitude are discussed in Refs. 1-6. At this time, it is generally assumed that operations at 130 km will be feasible, and there is some hope that the lower altitude of 100 km may be possible. Demonstration of deployment of a shorter tether of approximately 20-km length and a 23-kg satellite has been scheduled to occur in 1991, using an unmanned booster rocket as the carrier (Ref. 7). The more ambitious TSS-1 experiment involving an upward deployment of 20-km, and a satellite of 500 kg has been scheduled for 1992. Detailed planning for other experiments with longer tethers is being delayed pending the outcome of these 1991-92 trials.

The tethered sub-satellite to be used for aerothermodynamic experiments has been designated TSS-2, so the TSS identity is used as a generic term in the discussion to follow. Also, for brevity, we shall refer to the "satellite" interchangeably with sub-satellite in most places. At this time the TSS-2 configuration is assumed to be the same 1.6-m-diam sphere as used for TSS-1. Configurations of subsequent satellites have not yet been determined.

In anticipation of the successful outcome of the initial tethered satellite deployments, there was a desire to identify and describe specific experiments that might be conducted using TSS-2 and any follow-on satellites. The first author and a colleague, Professor F.C. Hurlbut, of the University of California at Berkeley, collaborated in recommending the experiments that were believed to be of high priority because of their technical value, their suitability for early implementation, and their probability of success under the expected conditions (Ref. 6). Some aerothermodynamic data of greatest interest for design of re-entry vehicles, e.g., rates of real gas chemical processes, are not given the attention that may be expected owing to the low density and probably frozen gas-phase processes at the planned TSS-2 orbiting altitude of 130 km (Ref. 8). Although such experiments are not emphasized for TSS-2, their priority would become high if significantly lower altitudes ($\approx$ 90 km) of TSS orbits prove feasible. Other experiments of potential value are not proposed because of the time needed in preparation or uncertainty of success.

With the discussions and recommendations of experiments already published in Ref. 6, the objective of this report is to give the results of several supporting analyses carried out as part of the study of potential aerothermodynamic experimentation with tethered sub-satellites conducted under NASA Research Grant NAG-1-878. These concern (1) a method for estimation of local and overall aerodynamic forces on bodies in transitional rarefied flow, (2) problems and possibilities of aerodynamic probes for determining various

atmospheric and flow- field properties under TSS conditions, (3) effectiveness of aerodynamic stabilization of TSS, and (4) optimum TSS shapes contributing to achievement of lower orbit altitudes and reduced flow disturbance.

AERODYNAMIC FORCES ON TETHERED SUB-SATELLITES

The overall size of the earlier sub-satellites is expected to be small; the TSS-1 and 2 currently discussed are 1.6-m-diam spheres with appendages of comparable dimensions, i.e., 1-2 m. At 130 km, using data from Ref. 9 for an exoatmospheric temperature of 800 K, Bird's "variable hard sphere" (Ref. 10) mean free path is 8.9 m, giving an overall Knudsen number of $Kn = \lambda / d = 5.6$ for $d = 1.6$ m. On the same basis, at 100 km altitude, $Kn = 0.056$. The tethers are expected to have diameters of only 1-3 mm, thus experiencing free-molecular flow at all of the altitudes considered. However, the overall Knudsen numbers of the 1.6-m-diam sphere indicate that pressure and shear on the surface of the sphere must be computed by a procedure for transitional flow. The assumption of free-molecular flow at the higher altitude of 130 km is justified for approximate calculations only. Therefore, some effort has been expended to develop a simple, transitional-flow method for estimating local pressure and shear. This will be useful for estimating forces and moments on the satellite and local conditions where instrumentation may be connected to the satellite surface.

The method of calculation is fully described in Ref. 11, so there is no need to present that material here. However, some examples of local pressure and friction coefficients computed for a 1.6-m-diam sphere orbiting at 7.5 km/s velocity with a surface temperature of 350 K at various altitudes are shown in Figs. 1a-1c. Velocity of the tethered satellite and other conditions obviously will vary for different altitudes. Assuming a spherical Earth of 6378-km-radius,

gravitational constant of 9.81 m/s^2, and a towing spacecraft orbiting at 220 km and 7.777 km/s with h = sub-satellite altitude in km,

$$U_\infty = 7.777\ (h + 6378) / (220 + 6378)$$

$$= 0.00118\ h + 7.518 \quad km/s \qquad (1)$$

Total drag coefficients as a function of altitude are shown in Fig. 2. Also shown in Figs. 1 and 2 are results for this case given in Ref. 8. The more sophisticated and accurate, but far more computation-intensive Direct Simulation Monte Carlo (DSMC) method was used in obtaining the data in Ref. 8. In light of the good agreement seen in Figs. 1-2, it is suggested that the simpler, quicker method of Ref. 11 is suitable for use in preliminary studies of TSS designs.

It is important to note that fully accommodated diffuse reflection of air molecules at the satellite surface has been assumed in regard to both normal and tangential momentum transfer in the calculations of Figs. 1-2. This is not a critical issue in predicting C_D when only spherical shapes are of concern, but it is a matter of much concern when local pressure and shear are calculated, or when lift and drag of many other possible satellite shapes are considered. Figures 3a and 3b, for example, illustrate the effect on local Cp and Cf corresponding to three different assumptions regarding the normal and tangential momentum accommodation coefficients (E) for the 1.6-m-diam sphere at 130-km altitude. A value of E= 0 in these calculations corresponds to an assumption of diffuse reflection of all molecules impacting and leaving the satellite surface. If completely specular interaction is assumed, then E = 1. There is evidence that E is influenced by the incidence angle, so that $E = E(\theta_i)$, with a tendency for E to be near 0 for near normal impact and near 1 for near grazing or tangential impact in a possible situation. Therefore, as an indication of how this type of variation of E may affect aerodynamic forces, a case is shown

where it is assumed that $E = \sin^6\theta$. This is an arbitrary but not unrealistic approximation to a phenomenon that is not well understood. The need for tethered satellite experiments on gas/surface interaction is a major theme in Refs. 1, 2, and 6.

Overall drag coefficients obtained in these calculations, for an altitude of 110 km, using the method of Ref. 11, are:

For diffuse accommodation, $C_D = 1.73$

For $E = \sin^6\theta$ accommodation, $C_D = 1.50$

For specular accommodation, $C_D = 1.54$

As stated above, much greater overall difference would be predicted for shapes such as slender cones, and the differences in local Cp and Cf are readily apparent in Fig. 3. It is seen that, although total drag of a sphere is not a sensitive indicator of the nature of gas/surface interaction, or even an average E, a local measurement of C_p or C_f at certain stations on a sphere would be much more interesting. Of even greater value would be the systematic measurements of momentum exchange described in Ref. 6.

The free-molecular-flow drag on the tether has been thoroughly analyzed in Ref. 12. Owing to the great length of tether of interest for reaching 100-130 km altitudes, the drag of the tether will exceed the drag of the 1.6-m-diam sphere considered herein. For example, if the towing vehicle is at 230 km and the 1.6-m- diam sub-satellite is at 130 km, depending on the particular set of atmospheric data and tether diameter, the drag on the sphere will be on the order of one Newton and the drag of the tether will be 10-20 times as large. Drag increases dramatically if much lower altitudes are considered because the air density increases roughly a factor of 10 for every 15-km decrease in altitude. Of course, weight of the TSS greatly exceeds aerodynamic drag at the contemplated altitudes.

PRESSURE/DENSITY/TEMPERATURE MEASUREMENTS

Data on ambient or freestream properties in the 90-130-km altitude range are of considerable interest, and it is not a simple task to obtain them. A significant problem is created by the flow field of the sub-satellite itself, and a second major obstacle is the uncertain knowledge of the composition of air at the time and place when measurements are made. Regarding the flow-field interference, Ref. 8 gives computed density, temperature, and air species fields which can be used to assess the problem. With specific reference to an altitude of 130 km, those computations show that chemical processes are essentially frozen throughout the flow field, so that air composition may be assumed constant. However, the results of Ref. 8 also show that the density and temperature in the flow for several meters upstream of the sphere are much different from the freestream static values. With regard to temperature, it is the translational temperature that changes, both rotation and vibration are essentially frozen.

We are concerned with the feasibility of obtaining useful data on flow-field and freestream properties by means of pressure measurements. Thus, it is not sufficient to merely record a signal from a pressure transducer, we have to know how to relate that signal to the pressure at a specified flow-field location. That entails procedures to account for rarefied flow within the pressure-probe plumbing from orifice to transducer and lag time of the system. Further, if there is hope to insert a probe into a region where freestream conditions exist, a probe system capable of reaching distances of order of 10 m from the 1.6-m-diam sphere is needed at 130- km altitude. Otherwise, computations will have to be relied on in attempting to extrapolate from close-in to freestream conditions.

First, the levels of pressures and the extent of the interference field are

investigated. It must be remembered that certain assumptions and approximations influence these results. For example, diffuse reflection and full accommodation of reflected molecules is the assumed gas/surface interaction model. A satellite outer surface temperature of 350 K and a pressure transducer temperature of 300 K are also assumed. Ambient conditions are taken from Ref. 9 for exoatmospheric temperature of 1200 K.

Treating the highly diffuse "shock layer" of the spherical satellite as a perfect gas with freestream constituents and using the results of Ref. 9, the static pressure, $p_l(x)$, along the stagnation streamline may be calculated as a function of x, the coordinate directed upstream from the forward stagnation point on the sphere. These are shown in Fig. 4. Then, by using Ref. 13, the pressures $p_t(x)$, that are predicted in the measurement device connected to a free- molecule impact pressure probe, e.g., an ion gauge, may be computed. Figure 5 gives some results of this exercise. It may be noted that ambient pressure, from Ref. 9, is $0(10^{-3})$ for this case. Predicted static pressures, $p_l(x)$, that would be measured within a transducer at various x-distances are given in Fig. 6 for a transducer temperature of 300 K and 130 km altitude. In both figures l = length of tubing from orifice to transducer and d = diameter of tubing. Because of strong thermal transpiration effects, the measured pressures, $p_l(x)$ and $p_t(x)$, differ greatly from the "true" static and impact pressures. These differences depend primarily on the thermal gradients across the pressure-sensing orifice and along the tubing connecting orifice to transducer and the length-to-diameter ratio of the tube. Orifice and tube inside diameters are assumed equal here.

Values of $x > 1$ m are not considered because that seems a likely upper limit on a fixed or simple traversing probe extending upstream of the forward stagnation point of the 1.6-m-diam sphere. Obviously, a more complicated and heavier mechanism could be devised to extend the probe upstream to greater

distances.

It is noted that the predicted impact pressure, within the transducer, is roughly constant with x and is between 10^{-4} and 10^{-3} torr, a range associated with ion gauges. Measured static pressures within 1 m or less distance is $0(10^{-4})$ torr within the transducer for the probe conditions assumed, so the same transducer could be used for both impact and static measurements.

The low pressures immediately cause concern regarding lag time in the response of the measurement system. At 130 km altitude it is appropriate to assume free-molecular flow in the orifice, tubing, and transducer, therefore the method of computing lag time follows Ref. 14. For this purpose, it is necessary to assign the volume of the measuring device, the length and diameter of tubing, orifice size, temperatures in the system, gas constant, and the initial and final pressures in the transducer. Diffuse reflection and full accommodation are assumed. The following results on lag time are based on a traversing probe having three different orifice and tube radii, a tubing length of 100 cm, and transducer volumes of 100 to 400 cc. Temperatures are taken to be 350 K at the orifice and 300 K at the transducer. By making the calculation for a given ratio of beginning and ending pressures, the results then apply to either impact or static pressure measurements.

Figure 7 gives the lag times for an arbitrary ratio of initial and final pressures of 0.8. The importance of plumbing size is very evident. Optimum tubing and orifice sizes are functions only of transducer volume, and are given below:

Transducer Volume (cc)	*Optimum Tubing & Orifice Radius (cm)*
100	2.6
200	3.3
300	3.8
400	4.2

These optimum radii are so large that they are not included in Fig. 7.

This review of the pressure measurement problem reveals that the level of the expected pressures and the lag time of the system do not seem to pose serious obstacles. It is clear that large theoretically-based corrections will be necessary to convert the recorded pressures to their corresponding values at the point in the flow field where the sensing orifice is located. These corrections are partly due to low- density flow phenomena within the pressure probe system and partly due to the interference field created by the satellite. The calculations have been made for conditions at 130-km altitude, because it is believed that the TSS-2 will be deployed to that altitude. Flow-field interference effects would be reduced at lower altitudes (cf. Ref. 8) but rarefied flow in the probe system would remain a factor.

Electron beam fluorescence is a technique for flow field surveys that seems applicable in the tethered satellite case. Recent reviews of the possibilities of such measurements in flight experiments are available in Refs. 15 and 16. Pioneering Canadian research (Ref. 17) has produced impressive results on atmospheric density and rotational temperature in the altitude range of 130 km by the use of electron-beam instrumentation on a sounding rocket. Later experiments by others are cited in Ref. 15. Thus, if not for TSS-2, later TSS should include electron-beam devices for surveying the flow field and, if feasible, probing into the free stream.

EFFECTIVENESS OF AERODYNAMIC STABILIZATION

There is an obvious reason for concern over maintenance of a desired satellite attitude and knowledge of variations in attitude when making flow-field measurements. Following from earlier remarks about the relatively low aerodynamic drag on the satellite, it is clear that aerodynamic stabilization can

only provide small restoring moments. However, "tail fins" may contribute usefully to the stabilization. An analysis of the degree of effectiveness of stabilizing by aerodynamic means follows.

Although flat-plate tail fins have been suggested by others, we have chosen to analyze a ring-tail stabilizer because it offers an equal amount of restoring moment for a given angle of attack in any plane. Obviously the tail moment arm, stabilizer area, and pre-set angle of incidence may be varied, but only one configuration is analyzed here. It suffices to quantify the magnitude of restoring moment that may be expected. Figure 8 shows the particular design chosen for calculations. Greater restoring moment could be achieved if larger values of L and R were assumed.

When angle of attack changes, some part of the stabilizer will be shielded by the spherical satellite. For simplicity, we have assumed that negligible force acts on the part of the ring tail in the "shadow" created in the flow by the sphere. This is indicated in Fig. 8. Also for simplicity, free-molecular flow is assumed in calculating forces for 130-km altitude. That is a very reasonable assumption for this calculation.

The pressure and fluid shear stress at stations on the circular ring tail are (cf. Ref. 18),

$$p_{fm}/p_\infty = [(1 + E)\, S_\infty\, (1 / \sqrt{\pi}) \cos\theta + 0.5\,(1\text{-}E)\, \sqrt{T_w / T_\infty}]\, \exp(-S_\infty^2 \cos^2\theta) + \{(1 + E)\,(0.5 + S_\infty^2 \cos^2\theta) + 0.5\,(1 - E)\, \sqrt{T_w / T_\infty}\, \sqrt{\pi}\, S_\infty \cos\theta\}\, [1 + \mathrm{erf}\,(S_\infty \cos\theta)] \qquad (2)$$

and

$$\tau_{fm}/p_\infty = [(1\text{-}E)\, S_\infty \sin\theta / \sqrt{\pi}]\, \{\exp(-S_\infty^2 \cos^2\theta) + \sqrt{\pi}\, S_\infty \cos\theta\, [1 + \mathrm{erf}\,(S_\infty \cos\theta)]\} \qquad (3)$$

The local value of θ, in radians, is

$$\theta = 1.5708 - \alpha \cos \beta \tag{4}$$

where $\cos \beta$ is treated as a positive quantity.

Increments of moment about the center of gravity of the satellite are given by

$$Mp = 2\ C\ L\ R\ p_\infty \int_0^{\beta_{max}} (p / p_\infty - 1) \sqrt{\cos^2 \beta}\ d\beta \tag{5}$$

$$M\tau = 2\ C\ R^2\ p_\infty \int_0^{\beta_{max}} (\tau / p_\infty) \sqrt{\cos^2 \beta}\ d\beta \tag{6}$$

where Mp is the contribution of pressure acting normal to the surface and $M\tau$ is the contribution of the shear acting tangentially to the surface of the ring. The integration proceeds from $\beta = 0$ to $\beta = \beta_{max}$, where

$$\beta_{max} = 3.1416 \text{ if } \alpha > \tan^{-1} (2R/L) \tag{7}$$

and

$$\beta_{max} = 1.5708 + \text{arc sin } [(L / R) (1 - \cos \alpha / \sin \alpha)] \tag{8}$$

when $0 < \alpha \leq \tan^{-1} (2R/L)$

A flare angle, or greater chord, radius, or moment arm may be specified in the tail design if added restoring moment is desired and if limitations on size permit. If rocket thrusters are used for control of the satellite, the potential interaction with aerodynamic control surfaces obviously must be considered.

Figure 9 gives the restoring moment calculated for an example in which the center of gravity is assumed to be at the center of the sphere, tail moment arm (from center of gravity to mid chord) is 1.6 m, tail chord is 0.4 m, tail radius is 0.8 m, and altitude is 130 km. Diffuse reflection has been assumed.

When lower orbital altitudes are involved, negative lift or down force may

be a primary aerodynamic design objective. In that case, satellite configuration may not be the sphere-with- stabilizer analyzed in this section, and transitional- rather than free-molecular-flow calculation procedures would apply. Reference 11 offers a procedure for such calculations, or, for more refined analysis, the DSMC method discussed in Ref. 8 could be used.

The further evaluate the magnitude of tail effectiveness that could be anticipated, it is interesting to briefly examine the response of a TSS to a disturbance that imposes a rotational motion on the body.

Dynamics of the satellite with a stabilizing tail may be examined in a simplified way by using the equation for plane motion of a rigid body rotating about a fixed axis with moment of inertia I and restoring moment M,

$$I \ddot{\alpha} = - M \tag{9}$$

The solution of Eq. (9), for small α, such that $\sin \alpha \approx \alpha$, and for $\alpha = 0$ at $t = 0$, is

$$t = (1/w_o) \int_0^{\alpha} d\alpha \, / \, \{1 - M \sin^2 (\alpha / 2) / (I w_0^2 \alpha)\}^{0.5} \tag{10}$$

If $M = K\alpha$, a good approximation, and if

$$\sin^2 (\alpha / 2) \leq I w_0^2 / (4 K)$$

or

$$\alpha_{max} = \sin^{-1} w_0 \sqrt{I / K} \text{ where } w_0 = (d\alpha / dt) \text{ at } t = 0, \tag{11}$$

then

$$t = 2 \pi \sqrt{I / K} \tag{12a}$$

A higher order approximation for t is

$$t = 2 \pi \sqrt{I / K} (1 + 0.25 \sin^2 (\alpha / 2) + \ldots) \tag{12b}$$

Treating the TSS as a sphere of uniform density, weighing 500 kg and having a 1.6-m diameter, an example of the predicted motion is given in Fig. 10. From Eq. (12) it is noted that the period is not affected by w_0, although the maximum amplitude is. The period in this example exceeds two minutes. It is expected that the c.g. of the tethered satellite will undergo motions imposed by its tether. The analysis described here only concerns the rotation of the satellite about its c.g., i.e., variation of angle of attack. This motion is of interest in connection with on-board experiments that may be affected by satellite angle of attack.

OPTIMIZED SATELLITE SHAPES FOR LOWER-ALTITUDE OPERATIONS

Previous discussion has concerned a 1.6-m-diam spherical satellite because it has been assumed that the first downward- deployed system will have that configuration. However, if later tethered satellites are used for atmospheric and aerothermodynamic measurements, lower orbital altitudes are certain to be desired. In that event, serious consideration must be given to the possibility of reducing the relative extent of the flow disturbance created by the satellite, i.e., the dimensions of the satellite's flow field. This is a concern if probing of freestream conditions is to be made easier. Another factor to consider is the possibility of generating useful levels of negative lift or down force to help the satellite penetrate to lower altitudes. Alternately, minimizing lift-to-drag (i.e., – L/D) could be a goal.

The aerodynamic characteristics of a non-spherical satellite were briefly examined to gain some appreciation of the change in shape and forces that could be expected. In view of the expected need to exert additional downward force to help maintain lower orbital altitudes and the desirability of a more pointed nose to minimize upstream flow disturbance, a right-circular cone split

along its horizontal plane of symmetry (i.e., a flat-bottom cone) was selected as the generic shape. For simplicity, a sharp nose was assumed, although at least a slight degree of blunting would be expected in a final design. Figure 11 is the sketch with nomenclature of this configuration and, Fig. 12 is an isometric view with the addition of wings that fold underneath the cone when not in use. Other constraints were as follow:

(1) zero angle of attack.

(2) volume equal to or greater than the 1.6-m-diam TSS sphere ($2.14 m^3$) but not more than 4 m^3

(3) maximum length of 4 m

(4) wing total area equal to cone bottom area

The approximate analysis procedure of Refs. 19-20 is very suitable for preliminary optimization or screening calculations of the type performed. Lift and drag coefficients were calculated by that method and combined with an optimization program (Ref. 21) to define flat-bottom cones producing "maximum" negative lift or down force at altitudes of 100 to 130 km under the constraints listed above.

To implement the procedure of Refs. 19-20, one must have lift and drag coefficients under both inviscid-flow and free-molecular-flow conditions. For the half-cone of Fig. 11, with area of the flat bottom taken as the reference area and assuming $S_\infty \sin\theta >> 1$, except on the flat bottom,

$$C_{Li} = -1.83 (\sin\delta)^{1.87} \tag{13}$$

$$C_{Di} = 0.915 \pi (\sin\delta)^{1.87} \tan\delta \tag{14}$$

$$C_{Lfm} = -(T_w \pi / T_\infty)^{0.5} (\sin\delta) / S_\infty \tag{15}$$

$$C_{Dfm} = \pi \sin\delta \{ \tan\delta \sin\delta + (T_w \pi / T_\infty)^{0.5} * (1/2S_\infty) \tan\delta + \cos\delta \} + \sqrt{\pi} / (2 S_\infty) \quad (16)$$

Following Refs. 19-20, parameters defined as

$$Pn_D = \sqrt{(U / \upsilon)_\infty s \sqrt{PFA / WA} (H_\infty / \{0.1 U_\infty^2 + 0.5 H_w\})^{0.63}} \quad (17)$$

and

$$Pn_L = Pn_D (PPA / PFA)^{0.25} \quad (18)$$

are calculated and used to obtain

$$C_D = (C_D) - C_{Di}) / (C_{Dfm} - C_{Di}) = \sqrt{2.6 / (2.6 + P_{nD1.6})} \quad (19)$$

and

$$C_L = (C_L - C_{Li}) / (C_{Lfm} - C_{Li}) = \sqrt{2.6 / (2.6 + Pn_{L1.6})} \quad (20)$$

Then, with Eqs. (13-16), values of C_D and C_L may be calculated. This procedure was programmed as a subroutine linked to the design optimization code (Ref. 21). Half-cone configurations meeting the given design criteria and producing the most-negative lift or ($- C_L A$) at each altitude were determined. Table 1 gives the results of this study. Note that it is the product of lift coefficient and reference area, not C_L alone, that matters in this case. It should also be noted that these results are affected by the particular constraints adopted, and the optimum shapes may change if these conditions are altered.

Table 1 presents characteristics of the flat-bottomed, sharp cones predicted to give greatest down force under the constraining conditions listed on the preceding page. The optimum shape, in all four cases, has the maxi-

mum specified volume of 4 m^3. Streamwise lengths are well below the maximum of 4 m that was allowed, but cone base radii and apex half-angles are relatively large. There is not much change in optimum shape as altitude varies.

Table 1

Optimized Shapes for Various Altitudes
when Volume = 4 m^3

Alt. km =	100	110	120	130
δ deg =	64.72	63.34	61.35	54.25
R_b m =	2.53	2.48	2.41	2.20
C_L =	- 1.16	- 0.83	- 0.51	- 0.085
C_D =	5.44	5.40	5.31	4.61
C_LA m^2 =	-3.48	- 2.57	- 1.61	- 0.30

To see the effect of changing the specified maximum volume, a case was calculated wherein the TSS-2 volume of 2.15 m^3 was taken as the maximum allowable. Table 2 gives those results, and it is seen that small changes in optimum proportions are indicated. The changes in apex angle are within the accuracy expected of the program, Again, the optimum and maximum allowed volumes are equal.

Table 2

Optimized Shapes for Various Altitudes
when Volume = 2.15 m^3

Alt. km =	100	110	120	130
δ deg =	63.93	62.50	60.57	55.05
R_b m =	2.03	1.99	1.94	1.80
C_L =	- 1.11	- 0.78	- 0.46	- 0.086
C_D =	5.24	5.23	5.18	4.75
C_LA m^2 =	-2.25	- 1.61	- 0.98	- 0.20

Figure 13 is a photograph of a model of the optimum shape of Table 1 for 100-km altitude. Wings that could be folded under the bottom of the half cone are shown in extended position. Their total area, A, equals the bottom or planform area of the half cone. Their optimum angle of attack also has been calculated, with the results shown in Table 3. Inasmuch as reference area for the wing C_L and C_D is the same as for the half-cone coefficients, the coefficients are additive. That is, neglecting any interference, with wings extended at 100 km altitude, $C_L = -1.16 - 0.49 = -1.65$, and $C_D = 5.44 + 1.17 = 6.61$ based on the area of the flat bottom of the half cone as the reference area.

Table 3

Optimized Wing Angles of Attack for
Sub-Satellite of 4 - m^3 Volume

Alt. km =	100	110	120	130
α deg =	- 53.2	- 52.2	- 51.2	- 49.0
C_L =	- 0.49	-0.33	- 0.19	- 0.10
C_D =	1.17	1.31	1.45	1.51

It was remarked earlier that decreased flow field disturbance is a desired feature of tethered satellites intended for collecting freestream data. Having found by means of the optimization study that half-cones giving maximum down force must have surprisingly high apex angles, and being aware that the forces generated aerodynamically by the sub-satellite body are rather minor compared to overall deployed weight and the drag on the tether, it may be more reasonable to simply design more slender shapes, half-cones or other bodies, to minimize flow disturbance and facilitate freestream surveying.

The possibility of determining freestream molecular speed ratio, pressure and temperature by use of a free-molecule pressure probe of the type shown in Fig. 14 was suggested in Ref. 6. It was shown that, if $S_\infty >> 1$ and free-

molecular-flow exists,

$$S_\infty = \{ 1/ (2 \sqrt{\pi})\}(p_1 / p_3) \sqrt{T_3 / T_1} \qquad (21)$$

where p_1 and T_1 are measured inside the orifice at $\theta = 0$, and p_3 and T_3 are measured inside of the orifice at $\theta = 90$ deg. The molecular speed ratio is defined as

$$S_\infty = U_\infty / (2 \Re T_\infty)^{1/2} \qquad (22)$$

where $\Re$ is the specific gas constant. Therefore, if the satellite's velocity is known from tracking, a value for $\Re$ is estimated from data in Ref. 9, and the probe pressures and temperatures are known from on-board measurements, S_∞ is given by Eq. (21). With S_∞ known, Eq. (22) gives T_∞. If T_∞ is known, p_∞ may be obtained from a second equation (see e.g., Ref. 6),

$$p_\infty = p_3 (T_\infty / T_3)^{1/2} \qquad (23)$$

Values of p_∞ and T_∞ obtained in this manner would supplement any other atmospheric data obtained. Although gas-gas or gas-surface chemical changes are not accounted for in Eqs. (21-23), it is probable that they will not obviate the pressure and temperature data at 130 km altitude. Implementation of this technique will require that the probe pictured in Fig. 14 meet the criteria for free-molecular flow and extend into the undisturbed flow. The first condition will be relatively easy to meet, but the latter will be far more easily met if a more slender satellite shape is used.

CONCLUDING REMARKS

The studies reported were a supportive part of a program intended to examine various facets of the tethered sub-satellite usage in future aerothermodynamic experiments. A relatively simple and accurate method for estimating lift and drag of shapes in transitional rarefied flow was formulated with partial support from this project. The feasibility of pressure measurement on and in the flow field of tethered satellites was analyzed. The effectiveness of aerodynamic stabilization of tethered satellites was explored, and a ring-tail design was offered as an alternate to the flat-plate stabilizers of TSS-2. A possible direction of future lower-altitude tethered satellite design was illustrated by coupling an aerodynamic estimation program with a design optimization program to define a series of shapes meeting specified criteria.

In addition to the work described in this report, contributions were made in the form of presentations, papers, and conference participation. These have been reported elsewhere. Pending the outcome of the initial flight trials and experiments with shorter tethers, it is uncertain how important the tethered satellite will become or how rapidly it will be exploited as a means for getting aerothermodynamic data under orbital and re-entry flight conditions. The body of preparatory knowledge in the form of analytical tools and assessments that has been developed will be useful when specific design issues are confronted.

ACKNOWLEDGMENTS

This work was accomplished with the support of NASA Research Grant NAG-1-878. NASA Technical Officers, at different times, were G. N. Wood, B. T. Upchurch, and R. DeLoach. Vanderbilt University undergraduate students who contributed significantly to various phases of the study are Paul A. Skoglund, Kimberly F. Sanland, Richard A. Kidd, and T. Ryder Booth. The authors are extremely grateful to all of these persons.

REFERENCES

1. Potter, J. L. and Hurlbut, F. C. "Aerothermodynamic Research With Tethered Satellites," Report of Aerothermodynamics Working Group, NASA Workshop, Menlo Park, CA, 7-9 Jan. 1987.

2. Wood, G. N. "Downward Deployed Tethered Platforms for High Enthalpy Aerodynamic Research," AIAA Paper 88-0688, Jan. 1988.

3. Hurlbut, F. C. and Potter, J. L. "The Downward Deployed Tethered Satellite: An Essential Element of New Aerospace Initiatives," A White Paper prepared at NASA request, 31 May 1989.

4. Wood, G. N., Wilmoth, R. G., Carlomango, G., and de Luca, L. "Proposed Aerothermodynamic Experiments in Transition Flow Using the NASA/ASI Tethered Satellite System 2, AIAA Paper 90-0536, Jan. 1990.

5. De Loach, R., Diamond, J., Finley, T., and Rhew, R. "End-Mass Instrumentation for the First SEDS/Delta II Mission," AIAA Paper 90-0537, Jan. 1990.

6. Hurlbut, F. C. and Potter, J. L. "Tethered Aerothermodynamic Research Needs," *Jour. Spacecraft and Rockets,* Vol. 28, No. 1, Jan. - Feb. 1991, pp. 50-57.

7. Crouch, D. S., Van Pelt, J. M. and Flanders, H. A. "A Titan II - Based Tethered Satellite System," IAF Paper 91- 004, Oct. 1991.

8. Dogra, V. K., Wilmoth, R. G. and Moss, J. N. "Aerothermodynamics of a 1.6-m-Diameter Sphere in Hypersonic Rarefied Flow." AIAA Paper 91-0773, Jan. 1991.

9. Jacchia, L. G. "Thermospheric Temperature, Density, and Composition: New Models," Smithsonian Astrophysical Observatory, Special Report 375, 1977.

10. Bird, G. A. "Definition of Mean Free Path for Real Gases," *Physics of Fluids,* Vol. 26, 1983, p. 3222- 3223.

11. Potter, J. L. and Peterson, S. W. "Local Bridging to Predict Aerodynamic Coefficients in Hypersonic, Rarefied Flow." submitted for publication in AIAA *Jour. Spacecraft and Rockets,* Aug. 1991.

12. Hurlbut, F. C. and Saldou, P. "Atmospheric Forces and Surface Temperatures on Tethered Satellites," Dept. of Mechanical Engineering, Univ. of California at Berkeley, 1990.

13. de Leeuw, J. H. and Rothe, D. E. "A Numerical Solution for the Free-Molecule Impact-Pressure Probe Relations for Tubes of Arbitrary Length," Institute of Aerophysics, University of Toronto, UTIA Report No. 88, Dec. 1962.

14. Schaaf, S. A. and Cyr, R. R. "Time Constants for Vacuum Gage Systems," *Journal of Applied Physics,* Vol. 20, No. 9, Sept. 1949, pp. 860-863.

15. Cattolica, R. J. "Modern Developments in Electron-Beam Fluorescence," in *Rarefied Gas Dynamics,* ed. by A. E. Beylich, VCH Publishers, Weinheim, Germany, and New York, N.Y., 1991, pp. 1581-1592.

16. Cattolica, R. J., Schmitt, R. L. and Palmer, R. E. "Feasibility of Non-Intrusive Optical Diagnostic Measurements in Hypersonic Boundary Layers for Flight Experiments,: AIAA Paper 90-0627, Jan. 1990.

17. de Leeuw, J. H. and Davies, W.E. R. "Measurement of Temperature and Density in the Upper Atmosphere Using an Electron Beam," *Canadian Jour. of Physics,* Vol. 50, 1972, pp. 1044-1052.

18. Bird, G. A. *Molecular Gas Dynamics,* Clarendon Press, Oxford, 1976, p. 93.

19. Potter, J. L. "Transitional, Hypervelocity Aerodynamic Simulation and Scaling," *Progress in Astronautics and Aeronautics: Thermophysical Aspects of Re-Entry Flows,* Vol. 103, ed. by J. N. Moss and C. D. Scott, AIAA, New York, 1986, pp. 79-96.

20. Potter, J. L. "Procedure for Estimating Aerodynamics of Three-Dimensional Bodies in Transitional Flow," *Progress in Astronautics and Aeronautics: Rarefied Gas Dynamics,* Vol. 118, ed. by E. P. Muntz, D. P. Weaver, and D. H. Campbell, AIAA, New York, 1989, pp. 79-96.

21. "Design Optimization Tools," a program licensed by VMA Engineering, 5960 Mandarin Ave., Suite F, Goleta, CA 93117.

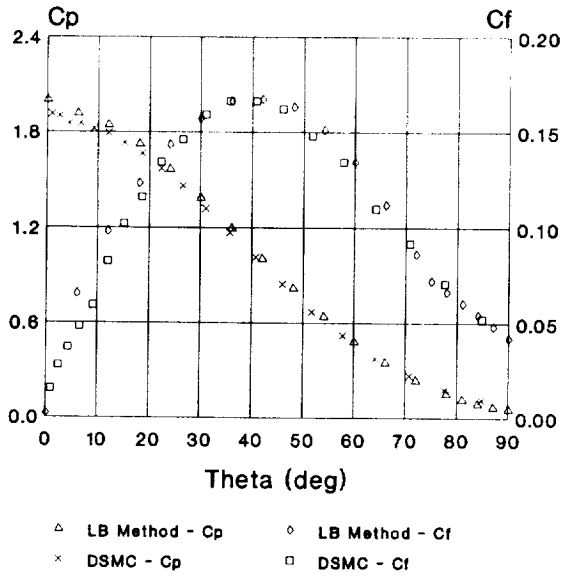

Figure 1a. Comparison of local shear and pressure coefficients on sphere at 90 km altitude.

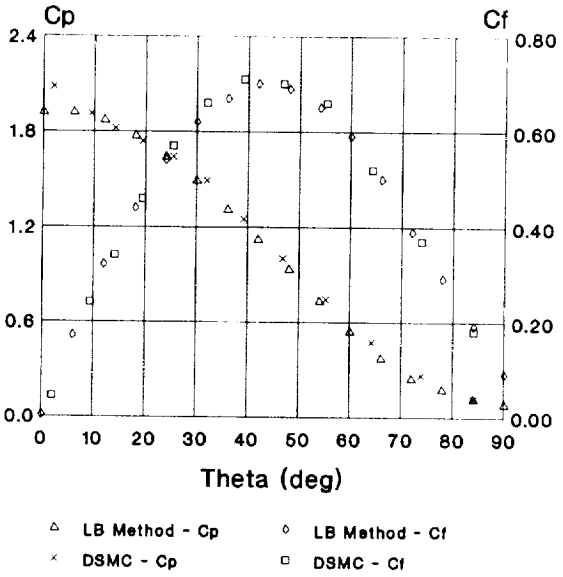

Figure 1b. Comparison of local shear and pressure coefficients on sphere at 110 km altitude.

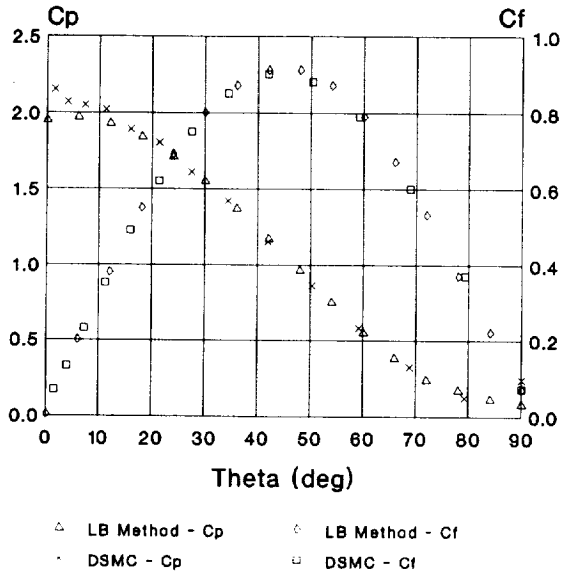

Figure 1c. Comparison of local shear and pressure coefficients on sphere at 130 km altitude.

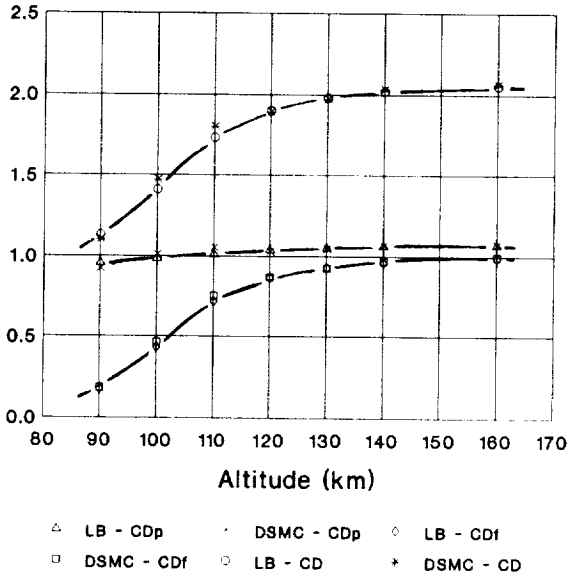

Figure 2. Comparison of sphere drag coefficients in transitional flow regime.

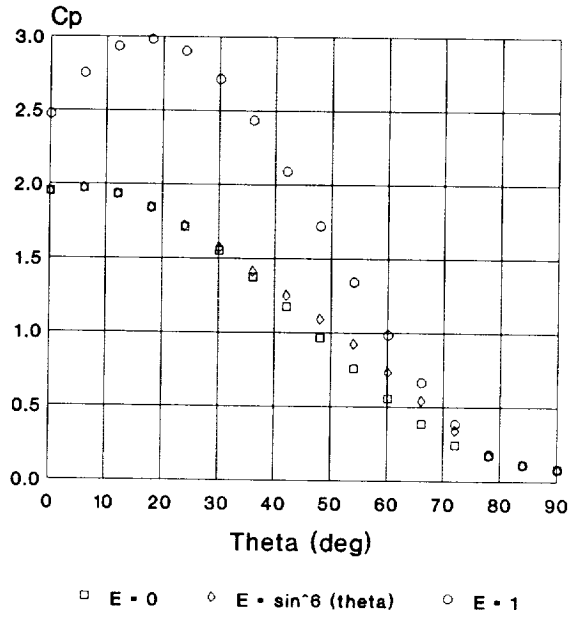

Figure 3a. Effect of momentum accommodation coefficient on Cp.

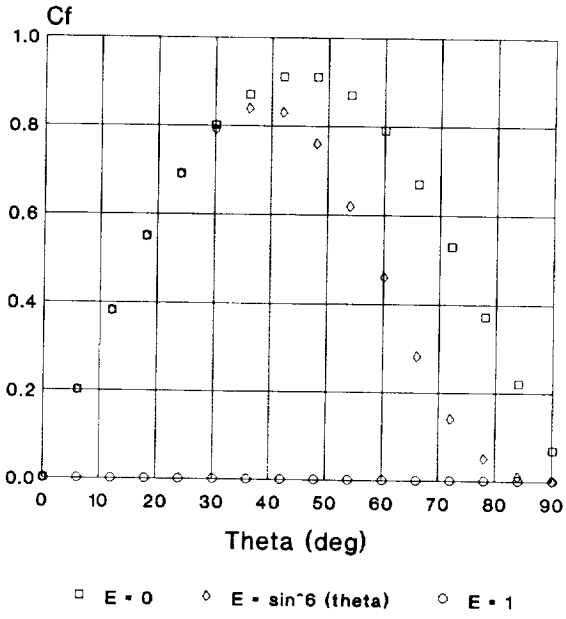

Figure 3b. Effect of momentum accommodation coefficient on Cf.

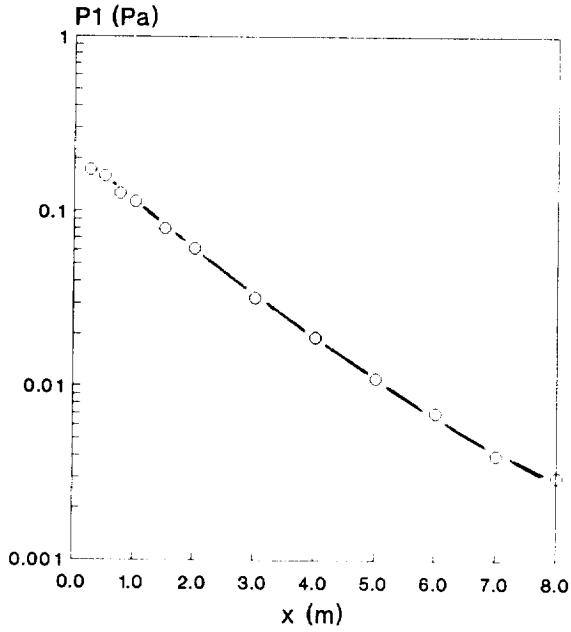

Figure 4. Predicted static pressure along stagnation streamline of TSS.

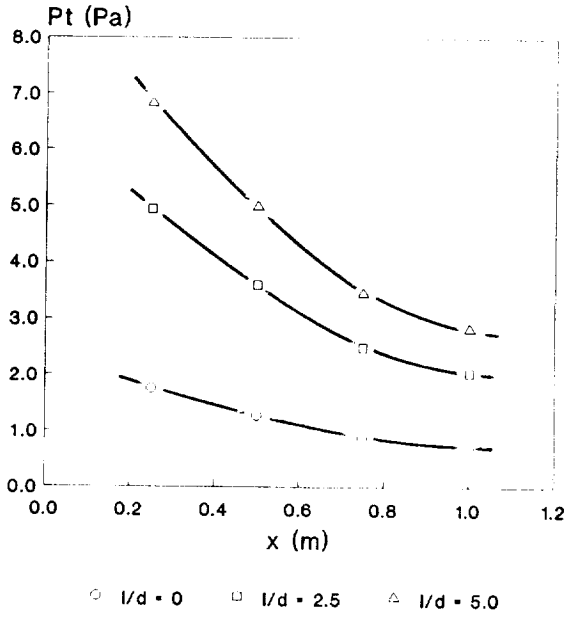

Figure 5. Predicted transducer impact pressure for three probe designs.

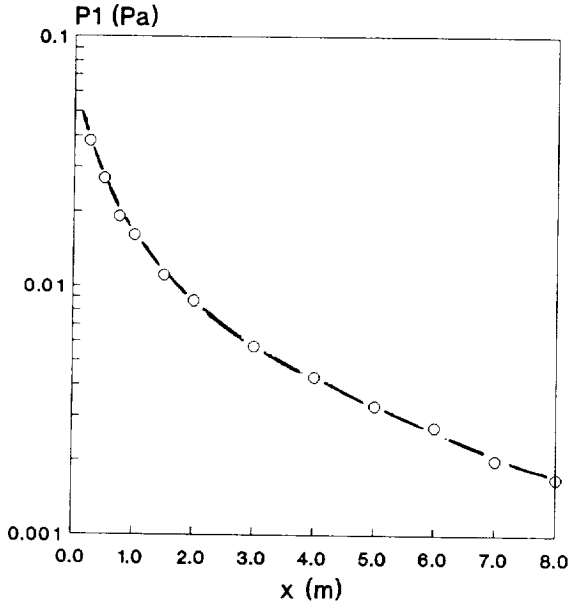

Figure 6. Predicted transducer static pressure along stagnation streamline of TSS.

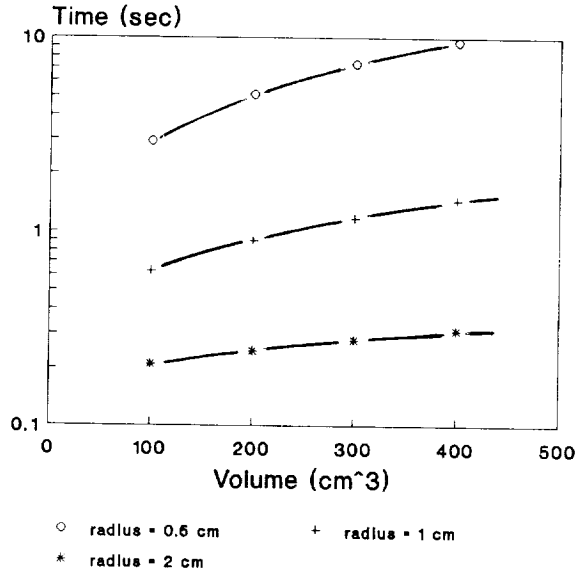

Figure 7. Response (lag) time of pressure measurement system at 130 km and P1/P2 = 0.8.

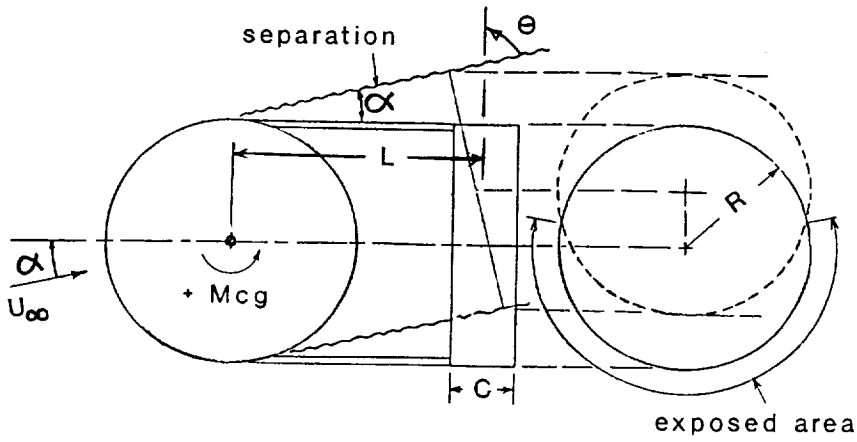

Figure 8. TSS with stabilizer (ring tail)

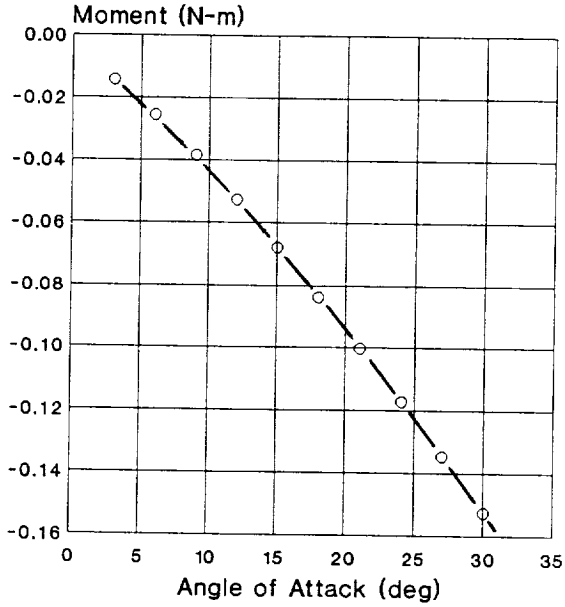

Figure 9. Restoring moment of ring tail of 0.4-m chord and 0.8-m radius at 130 km.

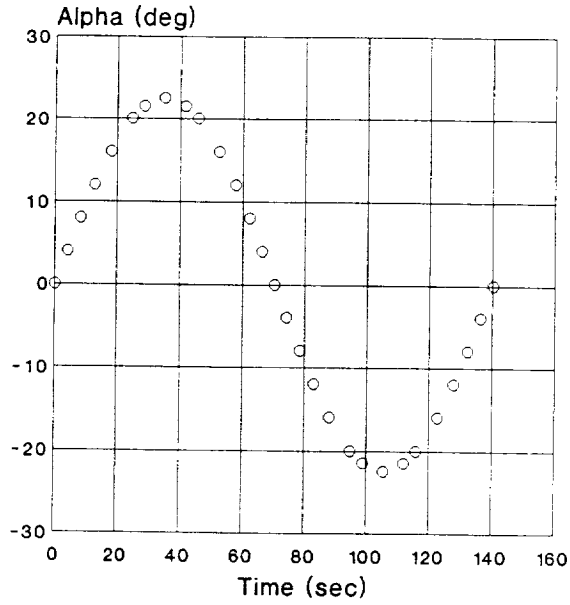

Figure 10. In-plane motion about C.G. resulting from 1-deg/sec disturbance at 130 km.

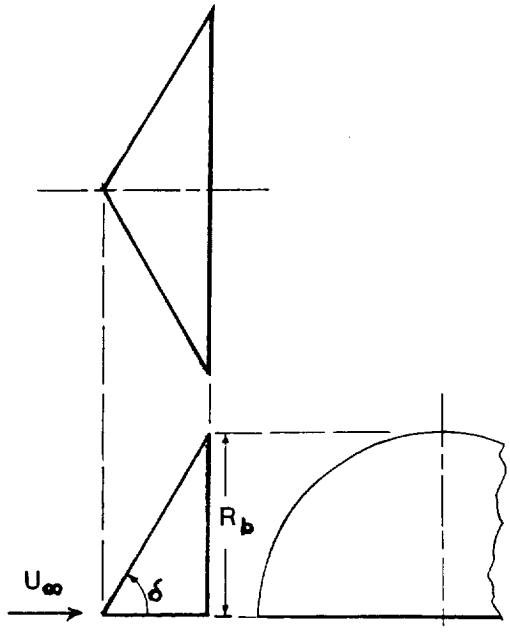

Figure 11. Flat-bottomed half-cone generic shape

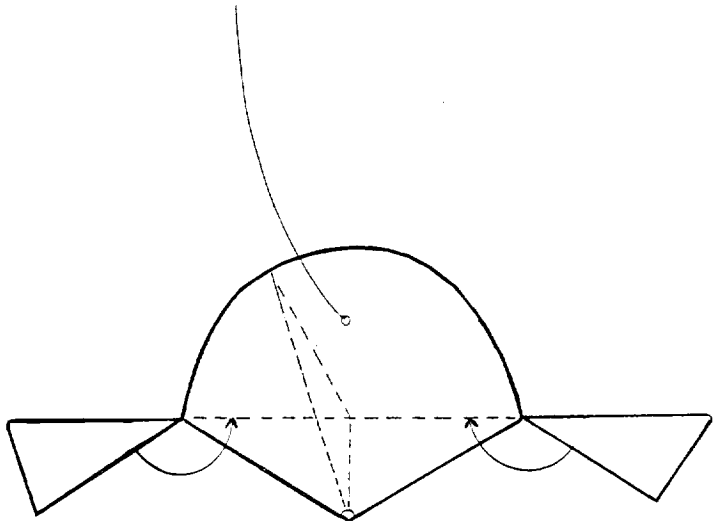

Figure 12. Isometric sketch of half-cone satellite

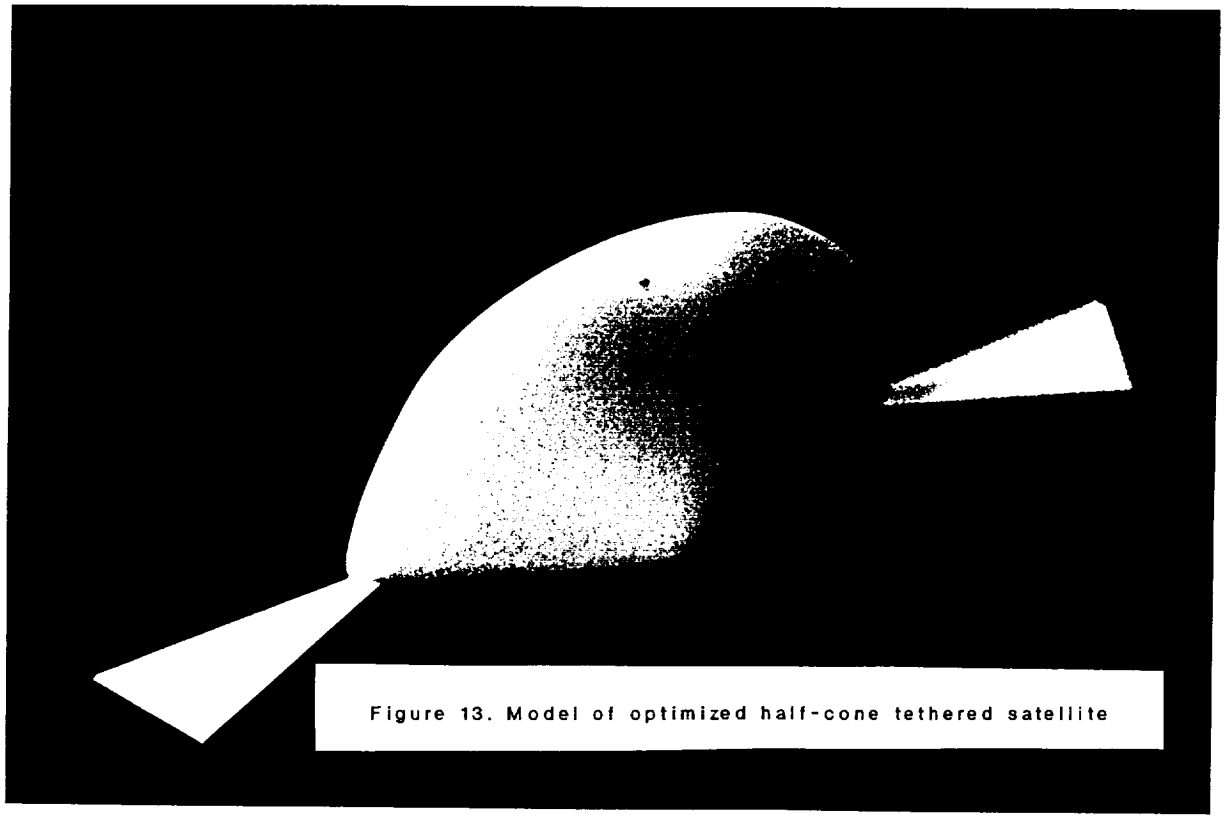

Figure 13. Model of optimized half-cone tethered satellite

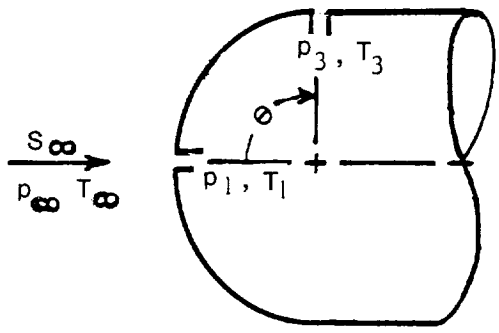

Figure 14. Free-molecule pressure probe